Isomeric yield ratios in proton-induced fission of ^{238}U

Z. Gao,* A. Solders,† A. Al-Adili, S. Cannarozzo, M. Lantz, and S. Pomp
Department of Physics and Astronomy, Uppsala University, 75120 Uppsala, Sweden

O. Beliuskina, T. Eronen, S. Geldhof, A. Kankainen, I. D. Moore, D. Nesterenko, and H. Penttilä
(IGISOL Collaboration)
University of Jyvaskyla, Department of Physics, Accelerator laboratory, P.O. Box 35(YFL), FI-40014 University of Jyvaskyla, Finland

(Received 12 October 2023; accepted 3 November 2023; published 30 November 2023)

Background: Isomeric yield ratios are an important observable in nuclear fission as they can guide model development by providing insight into the angular momentum generation. Furthermore, isomeric yield ratios are important in applications for nuclear energy, as well as in the study of the *r* process in stellar nucleosynthesis, and in the antineutrino mixing angle from reactor spectra. In nuclear data evaluations, the Madland-England model is commonly used to estimate isomeric yield ratios that have not been measured.

Purpose: To measure isomeric yield ratios in 25-MeV proton-induced fission of ^{238}U, and to compare the result with the values obtained from the Madland-England model and the fission model code GEF. Furthermore, to evaluate whether the predictions of GEF can be improved by coupling it to the nuclear reaction code TALYS.

Methods: Isomeric yield ratios in 25-MeV proton-induced fission of ^{238}U have been measured at the Ion Guide Isotope Separate On-Line facility. The excited state and the ground state were separated by mass using the phase-imaging ion-cyclotron-resonance technique in the double Penning trap JYFLTRAP. The number of counts of each state was extracted from the phase-images using a Bayesian Gaussian mixture model and, after corrections for detector efficiency and decay, the isomeric yield ratios were derived. The experimental values have been compared with the calculated results from the Madland-England model and the GEF code. Furthermore, GEF has been combined with the nuclear reaction code TALYS, in order to take advantage of the latter codes' implementation of the Hauser-Feshbach formalism, and the results have been compared with the experimental values.

Results: From the measurements, 19 new isomeric yield ratios in 25-MeV proton-induced fission of ^{238}U are reported and are, together with another 12 isomeric yield ratios (IYRs) from a previous campaign, compared with the model calculations. It is shown that, though the models manage to capture some of the features observed, there is room for improvement.

Conclusions: As predicted by the Madland-England model, a strong correlation between the measured IYRs and the spins of the long-lived states of the fission products is confirmed. However, the IYRs also vary between nuclides with the same spin-parity of the two states, and systematic trends in the IYRs of close-lying isotopes and isotones with similar nuclear configurations are observed. From the comparison of the experimental data with the prediction of GEF it is concluded that more data from proton-induced fission are needed to optimize the internal parameters of GEF. Furthermore, using a combination of GEF and TALYS in most cases results in an underestimation of the yield ratios. This might be explained by an underestimation of the angular momentum on the initial fission fragments by GEF. Altogether, these results highlight the possibility to use measurements of IYRs to improve model predictions and to study the angular momentum generation in nuclear fission.

DOI: 10.1103/PhysRevC.108.054613

I. INTRODUCTION

The isomeric yield ratio, referring to the relative yield of one of several long-lived nuclear states of a nuclide, is one of the observables of nuclear fission [1] which, through systematical investigations, can enhance our understanding of the fission process. Directly determined isomeric yield ratios of fission products from various systems [2–8] can be used to test and validate fission theory and fission models.

The isomeric yield ratios of fission products are also important as input parameters in the modeling of other processes. For example, the isomeric yield ratios of some fission products are important in the modeling of the *r* process in stellar nucleosynthesis [9] due to the significant difference of the half-lives and decay branching ratios of the isomeric states [9,10]. Another example is the study of the antineutrino mixing angle in reactor spectra, where isomeric yield ratios of certain fission products are needed as input parameters [11].

*zhihao.gao@physics.uu.se
†andreas.solders@physics.uu.se

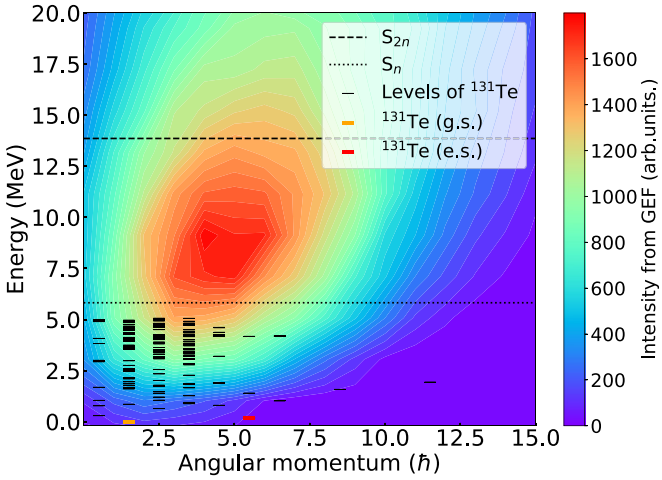

FIG. 1. Excitation energy vs angular momentum population of the primary fission fragment ^{133}Te, based on GEF calculations for ^{238}U(p, f) at 25 MeV. The one and two neutron separation energies of ^{133}Te are represented by a dotted and a dashed line, respectively. The partial level scheme with assigned spins of the de-excitation product ^{131}Te from the RIPL3 database [14] is added as short black lines. The long-lived excited state (e.s.) and the ground state (g.s.) of ^{131}Te are marked in red and orange, respectively.

In nuclear applications, isomeric yield ratios, together with other nuclear data, play a role in the design and optimization of nuclear reactors. The isomeric yields can potentially influence, for example, calculations of decay heat [12], as well as delayed neutron fractions and lifetimes.

In the fission process, the primary fission fragments (FFs), that are formed after the scission point, are highly excited. As an example, Fig. 1 shows a graphical representation of the excitation energy versus angular momentum population of the primary FF ^{133}Te. The figure is constructed based on the output of the GEF 2023/1.2 model [13] for the fission of ^{238}U induced by protons with kinetic energies of 25 MeV.

As seen in Fig. 1, the FFs cover a broad range of excitation energies, and a significant fraction of the fragments are above the one and two neutron separation energies. For these fragments, neutron emission is the most probable decay mode.

After, and in competition with, the neutron emission, continuous γ rays are emitted until the nuclei reach the discrete energy levels. In Fig. 1, the experimentally known discrete energy levels of ^{131}Te (one of the de-excitation products of ^{133}Te), as listed in the RIPL-3 database [14], are indicated as an example. While de-exciting, also the nuclear angular momentum will change due to the neutron and γ-ray emissions [15].

The decay goes on until a long-lived state is reached. From this point on, the nuclei are referred to as fission products (FPs). If a FP has more than one long-lived state, the relative population of those states are referred to as the isomer yield ratio (IYR). In this paper, the IYR is defined as the relative population of the high spin state to the yield of all observed long-lived states:

$$\mathrm{IYR} = \frac{Y_{HS}}{Y_{HS} + Y_{LS}}. \quad (1)$$

The IYR will depend on the initial angular momentum of the fission fragments, and can therefore be used as a probe for the angular momentum generation in fission. A simple model that is commonly used to estimate IYR in data evaluations of neutron-induced fission is the so-called Madland-England (ME) model [16]. In this paper we compare the measured ratios with those predicted by this model. We also compare the measured ratios with those predicted by the nuclear fission code GEF [13]. Finally, we derive the IYRs by coupling GEF to the nuclear reaction code TALYS [17], in order to take advantage of the latter's implementation of the Hauser-Feshbach de-excitation model.

Apart from the angular momentum of the fragments, the IYR also depend on nuclear properties of the FPs, such as the energy and spin levels, the nuclear deformations, the single-particle excitation, and configurations of the isomer pair. In cases where such information is available the correlation between the IYR and nuclear properties will be discussed.

In an earlier measurement at the Ion Guide Isotope Separate On-Line (IGISOL) facility [18], the phase-imaging ion-cyclotron-resonance (PI-ICR) technique [19] was used to determine the IYRs of Cd and In isotopes [8] in 25 MeV proton-induced fission of ^{238}U. In the present work, this data set is extended, adding another 19 IYR from the same fissioning system.

II. MEASUREMENT

The measurement procedure and the analysis routine have been thoroughly described elsewhere [20], and hence only a brief description will be given here.

Measurements of IYRs in proton-induced fission of uranium [^{238}U(p, f)] at a beam energy of 25 MeV were performed at the IGISOL facility. Fission products were separated based on their mass-to-charge ratio (m/q) by the IGISOL mass separator. After the separation, the ions of interest were cooled and bunched before injected into the double Penning trap JYFLTRAP [21]. In the first trap, the side-band cooling technique [22] was used to select the ions of interest, while the PI-ICR technique [23–25] was used to mass selectively separate the ions by nuclear states in the second trap, after which they were projected onto a position-sensitive microchannel plate (MCP) detector. The data consists of phase images of the ions in the two states. An example of such a phase image for ^{131}Te is shown in Fig. 2. To minimize a possible systematic error from an inhomogeneous detection efficiency of the MCP, several such phase images, with the two states in different positions, were usually recorded for each isomer pair. From all images for a specific pair, the populations of the two states were obtained using a Bayesian Gaussian mixture model to determine the probability of each event to belong to either of the two states or the background. After corrections for the detection efficiency and the decay of the fission products, the IYR was derived as the weighted average of the results from the different images, and the uncertainty was determined as the larger of the internal and external uncertainty. For a more detailed description of the data analysis, see Gao *et al.* [20].

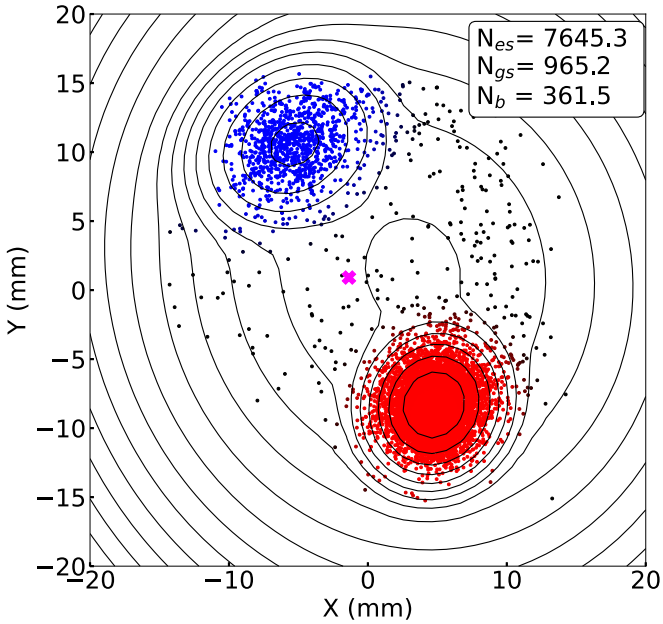

FIG. 2. Phase image for $^{131}Te^{+}$ ions obtained with PI-ICR technique. The color of the points represent which distribution each event belong to, the excited state (red), the ground state (blue), or the background (black). The magenta cross marks the central axis of the trap projected onto the MCP.

III. MODELING

Alongside the fast development of computer capacity, a huge improvement in fission modeling has been seen over the last decades. Several fission model codes, such as MCHF [26], CGMF [27], FIFRELIN [28], and FREYA [29] have been developed. Starting from the excited compound nucleus, these codes use assumptions on the division of nucleons, energy and angular momentum between the nascent fragments, in order to deduce the states of the fission fragments after scission. The subsequent de-excitation of the fragments, through neutron and γ-ray emission, is calculated using the Hauser-Feshbach formalism [30]. The resulting fission observables, such as neutron multiplicity, γ-ray multiplicity and fission yields, are then compared to measurements, and model parameters are optimized to fit the model to the data. However, these codes are in general not publicly available.

The GEneral description of Fission observables (GEF) [13] takes a more phenomenological approach in that it models the complete fission process with a large number of degrees of freedom, while still preserving all correlations. The free parameters are optimized against a large data set of fission observables, including IYRs. While GEF has a simplified de-excitation model compared to the above-mentioned codes, it is freely distributed and can hence easily be coupled to other codes.

A. The Madland-England model

In early articles [31,32], isomeric cross-section ratios observed in nuclear reactions, such as (n,γ) and (γ,n), were used to deduce the angular momentum distribution of the compound nucleus which was formed in the reaction, using a spin-dependent statistical method. This method was further developed and applied to the observed IYRs in fission, in order to deduce the angular momentum of primary fission fragments [2–6,8,16,33]. The Madland-England (ME) model [16] is based on that method, and the assumption that all fission fragments from a certain fission reaction carry the same average angular momentum. As in many other models, it is further assumed that the angular momentum of the fragments, J, follows the same Rayleigh distribution as the distribution of level densities [31,32],

$$P(J) \propto (2J+1)e^{\frac{-(J+0.5)^2}{2\sigma^2}}. \tag{2}$$

In this description, the so-called spin cut-off parameter σ determines the expectation value as well as the variance of the angular momentum, and is hence also directly linked to the root-mean-square of the angular momentum,

$$J^2_{\text{rms}} = 2\sigma^2 - \sqrt{0.5\pi}\sigma + 0.25 \approx 2\sigma^2. \tag{3}$$

Furthermore, a spin divider, J_c, is defined, and it is assumed that all fragments with angular momentum smaller than J_c will decay to the low spin state while fragments with higher angular momentum will decay to the high spin state. If there are FFs with angular momentum equal to J_c, those fragments will be divided equally between the two states. Using experimentally known IYR for specific fission reactions, the only parameter of the model, the J_{rms}, can be adjusted to those data and the model can be extrapolated to determine other IYR from the same reaction.

B. GEF

GEF is a fission code in which experimentally known fission observables are used to optimize the model performance. From a few user inputs, such as target nucleus and projectile type and energy, the model derives the probability of each fission channel and simulates the subsequent fission process. From the model calculation, the properties of the excited FFs after the scission point, including excitation energy and angular momentum, can be obtained. As in the Madland-England model, the angular momentum distribution is assumed to be described by Eq. (2).

To describe the emission of neutrons and γ-rays, GEF uses a simplified de-excitation model. Most importantly, the physics model assumes that the neutron and continuous γ-ray emission leaves the angular momentum of the nucleus unchanged, on average. The output of GEF contains information on various fission observables, such as fission product yields, neutron multiplicities, and γ-ray multiplicities. For FPs which have more than one long-lived state, the IYRs are also derived. Experimental yields are used to adjust the model's internal parameters and to validate the model performance [13]. Being a Monte Carlo model, the statistical uncertainty of GEF depends on the number of events simulated. In this work, all ratios from GEF were determined with a statistical uncertainty smaller than 1%.

C. GEF + TALYS

Because of the simplified handling of the de-excitation process in GEF, efforts were made to couple GEF with the nuclear reaction code TALYS [17]. In this approach, GEF is used to simulate the fission process until the formation of the FFs. The state of the fragments, more specifically their angular momentum and energy distributions, are then extracted from GEF (see Fig. 1) and fed directly to TALYS version 1.96, which handles the de-excitation process using the built-in Hauser-Feshbach formalism.

Due to the stochastic nature of the neutron emission, several FFs contribute to the yield of any particular FP, and hence, to the measured IYR. To account for this, TALYS calculations were performed for all FFs that decay to a specific FP, and the populations of the two states ($P_{\text{e.s.}}$ and $P_{\text{g.s.}}$) were extracted from the outputs. The contribution from each fragment was then weighted by each fragment's yield, according to GEF, to obtain the IYR.

In the TALYS calculations, both continuous and discrete energy levels of the fission fragments and products are needed as input data. For the discrete part, experimental data is used as far as they are complete. For example, for ^{131}Te there are 319 levels listed in the RIPL-3 database [14]. However, only 173 of those are assigned with spin-parities (presented as short lines in Fig. 1) and out of those, only the 35 lowest levels are considered to be complete (i.e. no intermediate levels are missing).

Between the experimentally known complete level scheme and the one-neutron separation energy, level density models have to be used to add discrete and continuous levels in order to produce a complete level scheme. TALYS comes with six different level density models implemented. In the present work, all six models were tested. However, the back-shifted Fermi gas model (BFM) [34] showed best agreement with the measurements and only results using this model will be presented here.

IV. RESULTS AND DISCUSSIONS

After analyzing the obtained phase images, 19 IYRs were determined and are presented in Table I. In one case, ^{127}In, three long-lived states were observed with spin assignments 1/2, 9/2, and 21/2. In this case, the experimental IYR and the one from GEF + TALYS is determined as the yield of the two high-spin states over the total. However, in GEF only the two lower spin-states are present, and the ME-model is only applicable to two long-lived states. In these cases, the IYR is determined from the two lower spin-states.

For the discussion, another 12 IYRs, from measurements by Rakopoulus *et al.* [7,8] using the same fission reaction, are also included in the table. Hence, the full data set includes 31 IYRs in 25-MeV proton-induced fission of uranium.

In the following sections we compare the results of the measurements with those obtained from the model calculations, and we will discuss the dependence of the IYRs on the nuclear structure of the FPs. In order to do so, the basic properties of the isomers, the spin-parity assignments and energy differences, as retrieved from NUBASE2020 [35] and the latest experimental publications [36–39], are included in Table I. Furthermore, in cases where such data are available, nuclear configurations of the measured states were retrieved from the nuclear structure database ENSDF [40] and presented in Table II.

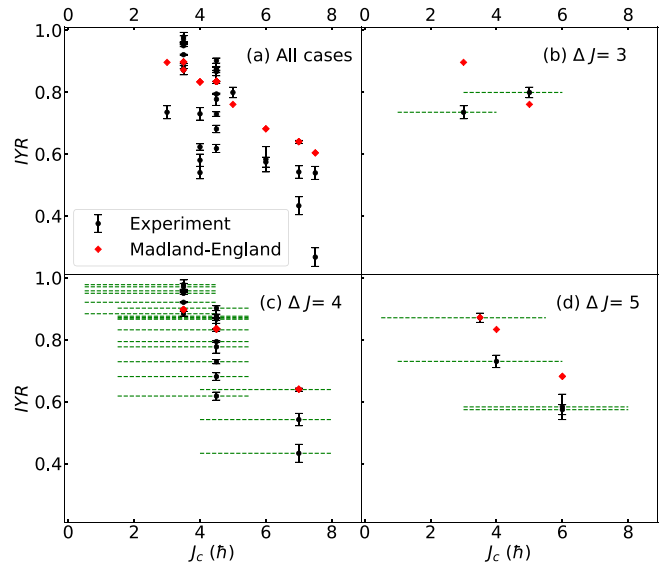

FIG. 3. The measured IYRs (black points) as a function of the spin divider J_c of the measured states are compared with the calculated IYRs (red diamonds) from the Madland-England model. (b) to (d) show the data conditioned on the spin difference between high and low spin states. Green lines represent the observed isomer pairs.

A. Dependence of the IYR on the spins of the isomers

The ME model was adjusted to the experimental data using a weighted least-square fit, resulting in a root-mean-square angular momentum of 10.5 $\hbar$. Panel (a) of Fig. 3 shows the resulting IYRs as a function of the spin divider J_c, together with the experimental values. As expected, a monotonically decreasing trend of the calculated IYR can be observed. The measured IYRs exhibit a similar trend, although with greater variations. Hence, it is fair to say that even though the ME model captures the overall trend, it cannot reproduce the measured data.

In the ME model, the spin divider is slightly adjusted depending on the parity of the spin difference between the high and low spin states, which is the reason why different J_c can result in similar IYR. However, this small adjustment cannot explain the average increase in the measured IYRs between $J_c = 4\,\hbar$ to $J_c = 4.5\,\hbar$ [panel (a) of Fig. 3].

In panels (b) to (d) of Fig. 3, the IYRs as a function of J_c are presented conditioning on the spin difference of the two states, and the dotted lines represent the spin difference between the high and low spin state. In panel (b), an opposite trend to what is predicted by the ME model can be observed, in that the IYR of ^{138}Cs is larger than the IYR of ^{102}Nb.

In panels (c) and (d) of Fig. 3 a general trend of decreasing IYR with J_c, predicted by the ME model, is observed in the data. However, the ME model fails to explain the rather big

TABLE I. The measured values of the IYRs together with the calculated ratios from the Madland-England model, the fission model GEF, and the combination of GEF + TALYS. The long-lived exited state of ^{127}Cd is missing the GEF database, and hence, no value is presented. For similar reasons, ratios marked with a dagger (†) were determined from two out of three long-lived states. The spin-parity assignments of the states and the excitation energy of the excited state are retrieved from the NUBASE 2020 database [35] unless stated otherwise. Spin parities put in parentheses means that the value is assigned based on experimental observations but is yet to be confirmed, while the flag ($^{\#}$) means that the value is based on theoretical predictions. Nuclides marked with a star (*) were measured by Rakopoulus *et al.* [7,8].

	Ground state	Excited state		IYR	IYR	IYR	IYR
Nuclide	I^{π}	E (keV)	I^{π}	measurement	ME	GEF	GEF+TALYS
^{102}Nb	(4^+)	94(7)	1^+	0.735(21)	0.896	0.965	0.672
^{119}Cd*	$1/2^+$	146.54(11)	$11/2^-$	0.871(15)	0.872	0.831	0.726
^{121}Cd*	$3/2^+$	214.86(15)	$11/2^-$	0.867(4)	0.835	0.757	0.559
^{123}Cd*	$3/2^+$	143(4)	$11/2^-$	0.876(7)	0.835	0.768	0.739
^{125}Cd*	$3/2^+$	186(4)	$11/2^-$	0.902(8)	0.835	0.783	0.792
^{127}Cd*	$3/2^+$	285(8)	$11/2^-$	0.87(4)	0.835	-	0.789
^{119}In*	$9/2^+$	311.37(3)	$1/2^-$	0.978(15)	0.897	0.963	0.903
^{121}In*	$9/2^+$	313.68(7)	$1/2^-$	0.971(11)	0.897	0.963	0.865
^{123}In*	$9/2^+$	327.21(4)	$1/2^-$	0.958(2)	0.897	0.963	0.893
^{125}In*	$9/2^+$	352(12)	$1/2^-$	0.950(3)	0.897	0.962	0.924
^{126}In	$3(^+)$	90(7)	(8^-)	0.574(16)	0.682	0.643	0.445
^{127}In*	$9/2^+$	394(18)	$1/2^-$	0.921(2)	$0.897^{\dagger}$	$0.958^{\dagger}$	0.866
		1770(40)	$(21/2^-)$				
^{128}In [36]	$(3)^+$	285.1(25)	(8^-)	0.583(4)	0.682	0.517	0.454
^{129}In [37]	$(9/2^+)$	447(13)	$(1/2^-)$	0.884(8)	0.897	0.948	0.661
^{128}Sn*	0^+	2091.50(11)	7^-	0.580(20)	0.833	0.585	0.455
^{129}Sn	$3/2^+$	35.15(5)	$11/2^-$	0.777(20)	0.835	0.815	0.799
^{130}Sn*	0^+	1946.88(10)	7^-	0.540(20)	0.833	0.544	0.471
^{131}Sn	$3/2^+$	65.1(3)	$11/2^-$	0.681(12)	0.835	0.727	0.591
^{129}Sb	$7/2^+$	1851.31(6)	$(19/2^-)$	0.539(21)	0.604	0.399	0.444
^{132}Sb	$(4)^+$	150(50)	(8^-)	0.433(29)	0.640	0.478	0.340
^{134}Sb	(0^-)	279(1)	(7^-)	0.625(10)	0.833	0.735	0.670
^{129}Te	$3/2^+$	105.51(3)	$11/2^-$	0.832(4)	0.835	0.819	0.673
^{131}Te	$3/2^+$	182.285(18)	$11/2^-$	0.867(14)	0.835	0.776	0.783
^{133}Te	$3/2^{+\#}$	334.26(4)	$(11/2^-)$	0.794(2)	0.835	0.716	0.726
^{132}I	4^+	110(11)	(8^-)	0.542(20)	0.640	0.651	0.632
^{133}I	$7/2^+$	1634.148(10)	$(19/2^-)$	0.267(30)	0.604	0.400	0.402
^{134}I	$(4)^+$	316.49(22)	$(8)^-$	0.639(5)	0.640	0.530	0.612
^{136}I	(1^-)	206(15)	(6^-)	0.730(20)	0.833	0.684	0.692
^{133}Xe	$3/2^+$	233.221(15)	$11/2^-$	0.618(13)	0.835	0.817	0.796
^{135}Xe	$3/2^+$	526.551(13)	$11/2^-$	0.729(7)	0.835	0.766	0.761
^{138}Cs	3^-	79.9(3)	6^-	0.799(17)	0.760	0.719	0.790

variations of the IYR for isomers with the same J_c. Two possible reasons for this variation are nuclear structure, and the angular momentum of the FFs. For example, the IYRs at $J_c = 4.5\,\hbar$ in panel (c) are observed in different nuclides with different nuclear structures. However, in some cases the nuclear structure is very similar, while a systematic variation in the measured IYR is still observed. A possible reason for this variation is thus that the angular momenta of the primary fission fragments are isotope dependent, as observed by Rakopoulos *et al.* [8].

B. Comparison with the models

An overall comparison between the model calculations and the experimental data is presented in Fig. 4. A general trend of underestimation of the yield ratio in the symmetric region (A = 119–125) can be observed for all models. In the high mass peak ($A > 130$) the Madland-England model seems to overestimate the population of the high spin state, while the GEF results are closer to the measured values. The combination of GEF+TALYS seems to lead to an underestimation of the IYR for most fission products, with a weighted root-mean-square deviation between the calculation and the experimental result of 0.10. The corresponding values for the ME model and stand-alone GEF are both 0.06.

The fact that the combination of and TALYS leads to an overall underestimation of the yield ratios could be explained by the different treatments of the de-excitation process used by the two codes. The GEF spin-energy population matrix that describes the FFs is optimized to reproduce experimental data, assuming that the angular momentum (on average) does not change until the nuclei reach the discrete energy levels. However, the same assumption seems not to be true for TALYS. It has, for example, been shown that the Hauser-Feshbach

TABLE II. Configurations of the observed high-spin and low-spin states of the fission products retrieved from the ENSDF database [40]. Positions left empty means that no data are available.

Isotopes	Low-spin state	High-spin state
Even-N In	$\pi p_{1/2}^{-1}$	$\pi g_{9/2}^{-1}$
Odd-N In	$\pi g_{9/2}^{-1} \otimes \nu d_{3/2}^{-1}$	
Even-N Sn		$\nu 2d_{3/2}^{-1} 1h_{11/2}^{-1}$
Odd-N Sn	$\nu 2d_{3/2}$	$\nu h_{11/2}$
^{129}Sb		$\pi g_{7/2} \otimes \nu h_{11/2} \otimes d_{3/2}$
^{132}Sb	$\pi g_{7/2} \otimes \nu d_{3/2}^{-1}$	$\pi g_{7/2} \otimes \nu h_{11/2}^{-1}$
^{134}Sb	$\pi g_{7/2} \otimes \nu f_{7/2}$	$\pi g_{7/2} \otimes \nu f_{7/2}$
^{129}Te	$\nu 2d_{3/2}$	$\nu h_{11/2}$
^{131}Te	$\nu h_{3/2}^{-1}$	$\nu h_{11/2}^{-1}$
^{133}Te	$\nu d_{3/2}^{-1}$	$\pi g_{7/2}^{2} \otimes \nu h_{11/2}^{-1}$
^{133}I	$\pi g_{7/2} \otimes g_{7/2}^{2}$	$\pi g_{7/2} \otimes \nu h_{11/2}^{-1} d_{3/2}^{-1}$
^{134}I		$\pi g_{7/2} \otimes \nu h_{11/2}^{-1}$
^{136}I		$\pi g_{7/2}^{2} d_{5/2} \otimes \nu h_{7/2}$
^{133}Xe	$\nu d_{3/2}^{-1}$	$\nu h_{11/2}^{-1}$

formalism implemented in the CGMF code results in a change in spins due to neutron and statistical γ-ray emission of the order of 3.5–5 $\hbar$ [15].

The most common spin assignment of the two states in this measurement is 3/2 and 11/2. To test to what degree the population of states could be explained by the spins of the two states, the IYR of all fission products with this particular configuration is presented in Fig. 5. The fact that the measured values span from 0.62 to 0.90 demonstrates the shortcoming of the ME model, and supports the observation by Sears *et al.* that the IYR of a particular fission reaction can not be determined solely from the spins of the states [41]. Behind this assumption in the ME model is the idea that the electromagnetic transitions will be strongest for minimum change in angular momentum, while at the same time ignoring change in angular momentum from neutron emission. Hence, this description is likely to be false.

GEF and GEF + TALYS, on the other hand, better manage to capture the variations in IYR, although both models generally underestimate the ratios.

C. Nuclear structure

The nuclides in Fig. 5 are all even-Z odd-N nuclei. This means that their nuclear structures, to some degree, are similar. For example, in most cases, one valence neutron orbit dominates the nuclear configurations at the high and low spin states (see Table II). Besides the similarity, one can observe differences in nuclear structures, such as different nuclear configurations of the low spin states for the tin, tellurium, and xenon isotopes. One proton pair breaking is observed in the high spin state of ^{133}Te that is not observed for other high spin states. Those observed differences in nuclear structures might contribute to the wide variation of the IYRs.

D. ^{102}Nb

The isomeric yield ratio of ^{102}Nb was measured for the first time. The obtained value of 0.735(21) is significantly lower than the values obtained from both the ME model and GEF, while the combination GEF + TALYS gives a slightly better result. Considering that very few levels of ^{102}Nb, as well as of the niobium fission fragments contributing to the ratio,

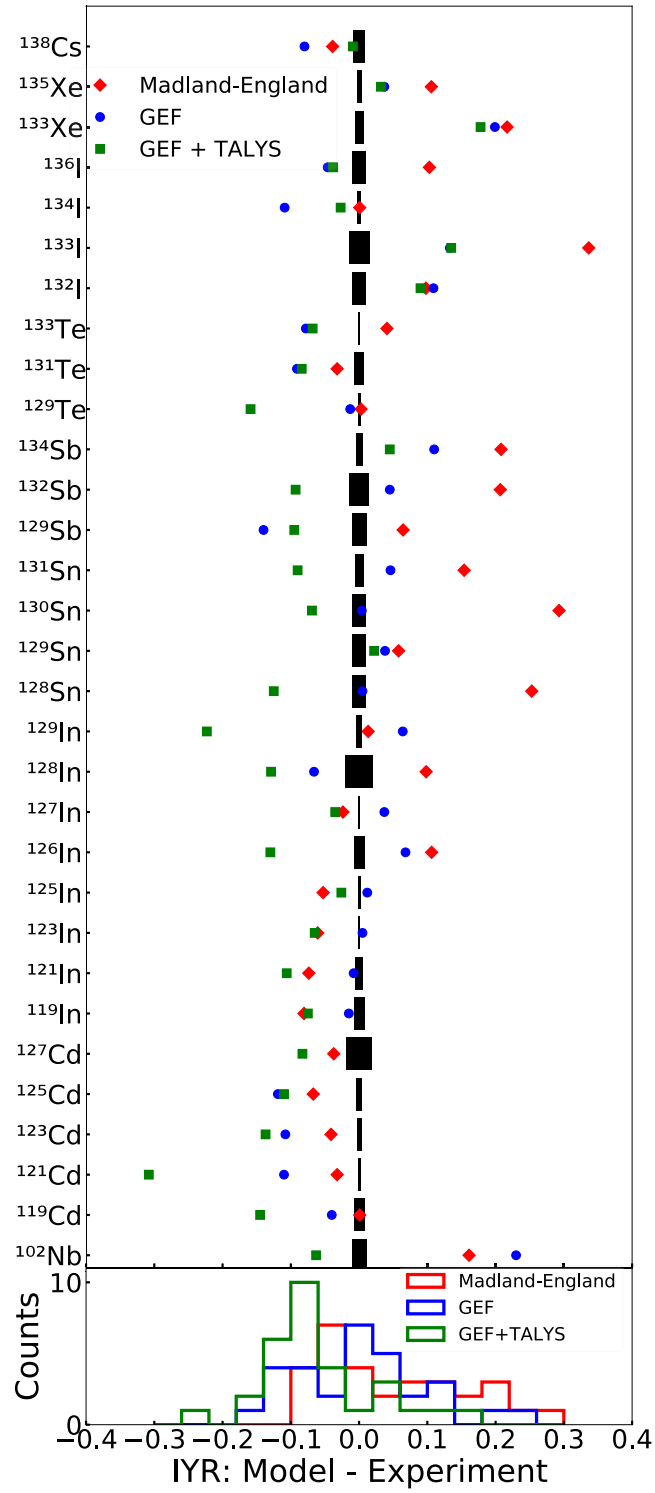

FIG. 4. Deviation between model calculations and the experimental values of the IYRs. The black boxes represent the one sigma uncertainties of the measured values.

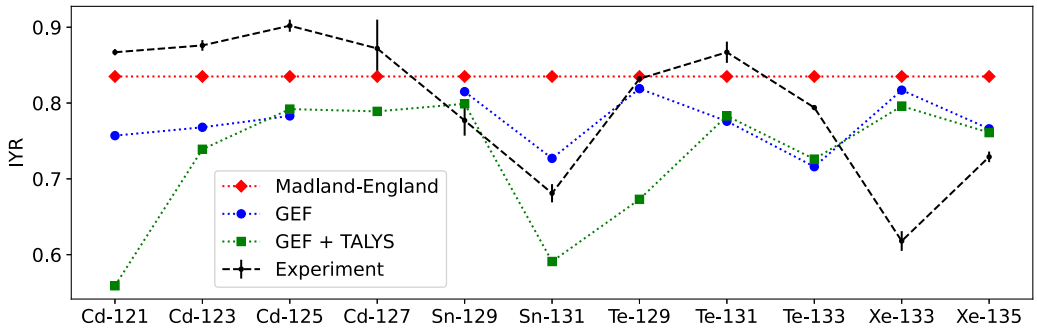

FIG. 5. The IYRs for all measured fission products for which the high spin is 11/2 and the low spin 3/2. The long-lived exited state of ^{127}Cd is missing in the GEF database, and hence, it does not give a value for this ratio. The dotted lines are to guide the eye.

are available in the ENSDF database [40], such discrepancies between measurement and calculations are not surprising.

According to Sonzogni *et al.* [11], ^{102}Nb is one of the main contributors to the antineutrino spectrum in the thermal fission of ^{239}Pu. This has been confirmed in a recent publication, showing that the β decays of both long-lived states have an important impact on the summation calculation of reactor antineutrino spectra [42]. Hence, the measured IYR presented here, although for a different reaction, could help to improve the calculations of the antineutrino spectrum.

E. Cadmium isotopes

The IYRs of the cadmium isotopes were measured in an earlier campaign. In Fig. 6 the result is compared to the model calculations. Except for the lightest isotope, all of the nuclei have the same spin-parity of the two states. As a result, the ME model predicts a constant IYR, quite similar to the experimental result. The ratios predicted with GEF and GEF + TALYS show more variation and are also, on average, further from the experimental results.

F. Indium isotopes

For the indium isotopes (Fig. 7), a strong neutron number parity effect of the IYR is observed. This coincides with a significant difference between the spin-parities of the even-N and odd-N isotopes. The very high spin ($8\hbar$) of the excited state odd-N indium isotopes results in significantly lower IYRs. This general trend is reproduced by all the models, although not in absolute numbers.

The even-N isotopes of indium are particularly interesting as they all have the same spin-parity of the two states. In fact, they even share the nuclear configuration in which one valence proton hole dominates the nuclear excitation from the ground to the excited state. As a result, the stand-alone models both predict the IYR to be constant. However, in the experimental data a clear trend of decreasing IYR with increasing mass is observed which cannot be explained by the nuclear structure. This could instead be an indication of a systematic variation in the angular momentum of the initial fragments with increasing mass number. If this assumption holds, it means that the angular momentum of the fission fragments varies, even between close-lying isotopes of the same elements. However, further modeling is necessary to understand this behavior.

G. Tin isotopes

In the case of tin, GEF reproduces the measured IYRs with remarkable precision, especially for the even-N masses (Fig. 8). The ME model, on the other hand, completely misses

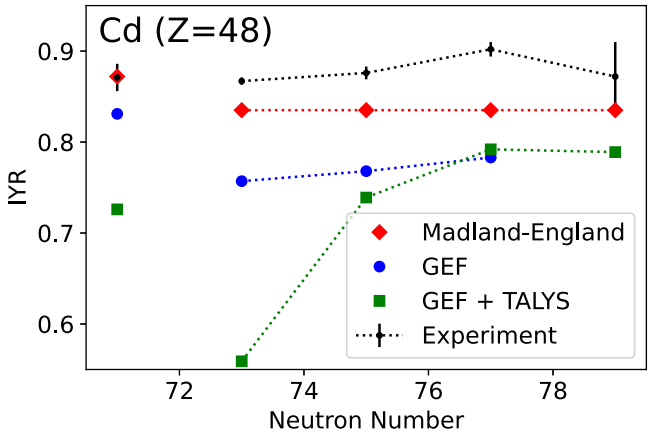

FIG. 6. The IYRs as a function of neutron number for the cadmium isotopes. The dotted lines connect isotopes for which the spin-parity of the two states are the same.

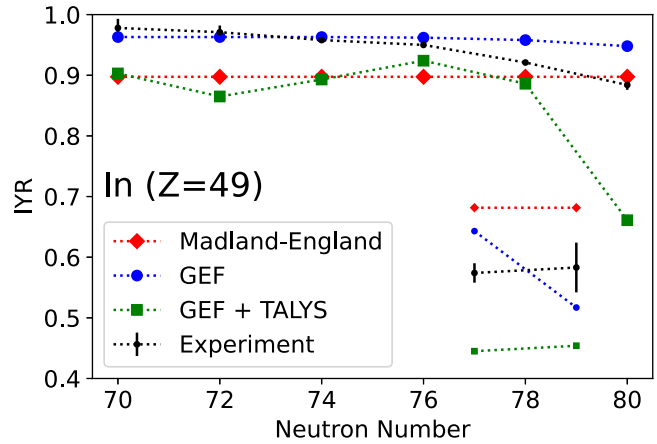

FIG. 7. The IYRs as a function of neutron number for the indium isotopes. The dotted lines connect isotopes for which the spin-parity of the two states are the same.

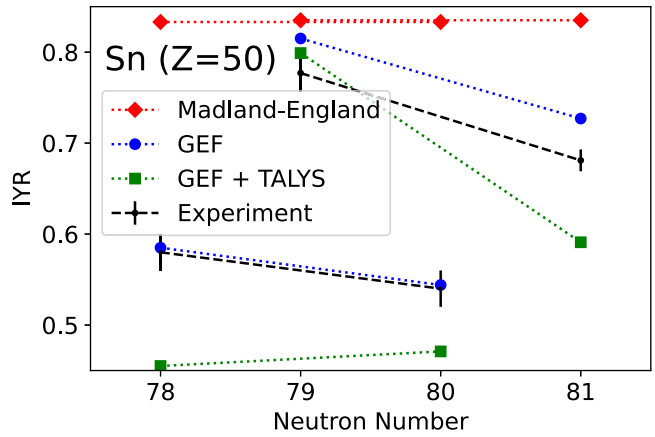

FIG. 8. The IYRs as a function of neutron number for the tin isotopes. The dotted lines connect isotopes for which the spin-parity of the two states are the same.

the difference in the yield ratios between the even-N and odd-N isotopes.

It can further be noticed that also in this case the yield ratios for isobars with the same spin-parity differ. In the case of the odd-N tin isotopes the two states even have the same nuclear configuration, both have one valence neutron dominating the nuclear structure. This is again an indication that the angular momenta of the corresponding fragments are likely to be different, even for isotopes of the same element.

H. Antimony isotopes

The odd-N antimony isotopes (Fig. 9), due to the neutron shell closure at $N = 82$, have very different nuclear configurations. In fact, none of the measured antimony isotopes share the same spin, and as expected the IYR does not show any systematic trends.

I. Tellurium isotopes

In the case of tellurium (Fig. 10), the three measured isotopes all have odd neutron numbers and all have the same

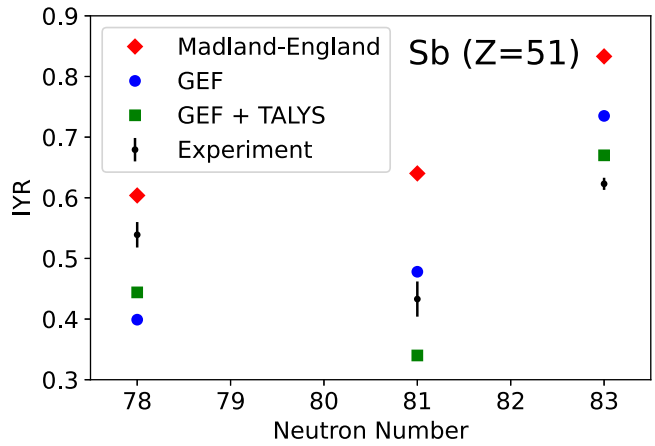

FIG. 9. The IYRs as a function of neutron number for the antimony isotopes.

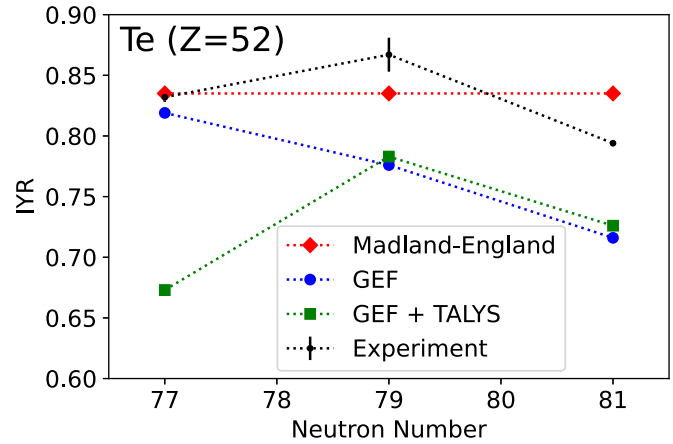

FIG. 10. The IYRs as a function of neutron number for the tellurium isotopes. The dotted lines connect isotopes for which the spin-parity of the two states are the same.

spin-parity of the states, however none of them share the same nuclear configuration. While the ME model predicts the average ratio of the isotopes correctly, it fails to replicate the details. Again this shows that the spins of the two states are not enough to predict the yield ratio. For these isotopes, also GEF fails to reproduce the ratios and the combination of GEF and TALYS does not do much better, although it seems to be better at capturing the trend.

J. Iodine isotopes

Due to the neutron shell closure at $N = 82$, the nuclear structure of ^{134}I and ^{136}I are significantly different and they also have different spin-parities of the two states. It is hence not a surprise that their IYRs differ. However, the isotopes ^{132}I and ^{134}I do share the same spin-parities and still the difference in the measure ratios are of the same order. None of the models used in the comparison manages to reproduce the observed trends (Fig. 11).

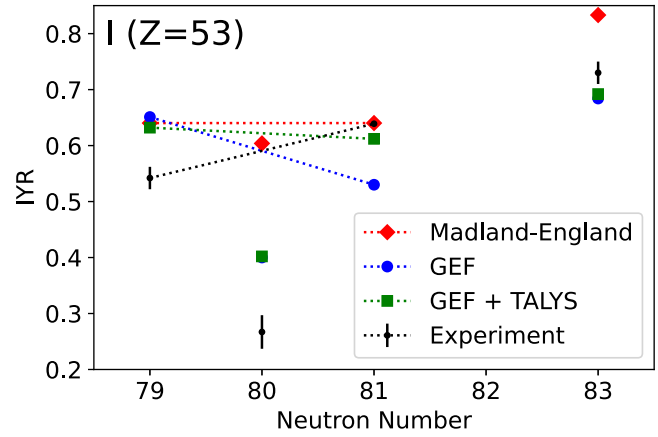

FIG. 11. The IYRs as a function of neutron number for the iodine isotopes. The dotted lines connect isotopes for which the spin-parity of the two states are the same.

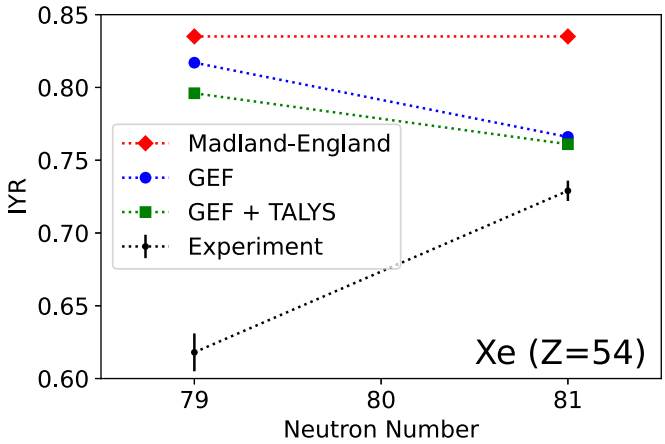

FIG. 12. The IYRs as a function of neutron number for the xenon isotopes. The dotted lines connect isotopes for which the spin-parity of the two states are the same.

K. Xenon isotopes

The two xenon isotopes in this study have the same spin-parity of the states, $3/2$ and $11/2$. As a result, the ME model predicts the same IYR (Fig. 12). All three models overestimate the yield ratio and none of them get the trend of increasing IYR with neutron number correct.

L. ^{138}Cs

Only one IYR has been measured for caesium isotopes, and therefore no observations can be made regarding trends. While GEF underestimates the value by more than 3σ, GEF + TALYS reproduce the value within the uncertainty of the measurement.

M. Proton number parity

In the results presented above, a strong even-odd effect of the measured IYR of isotopes of the same element is observed (see Figs. 7 and 8), which can be attributed to the neutron number parity. A similar behavior can be observed for the proton number parity in Figs. 13 and 14, where the IYRs of the $N = 79$ and $N = 81$ isotones are presented as a function of proton number.

For $N = 79$, the high-spin and low-spin states of the four measured even-Z isotones are assigned with the same spin-parity of $11/2^-$ and $3/2^+$. Hence, there are likely other explanations than the nuclear structure of the fission products for the observed variation in IYR of these isotones. One possibility is that the angular momentum population of the contributing fission fragments vary with proton number.

For $N = 81$, the even-Z isotones all have the same spin-parity, and the same is true for the odd-Z isotones. The systematic difference between the IYRs of the even-Z and odd-Z isotones again points to the importance of the nuclear structure in the population of the states, while the variation within the respective ensemble suggests that also the angular momenta of the primary fragments play a role.

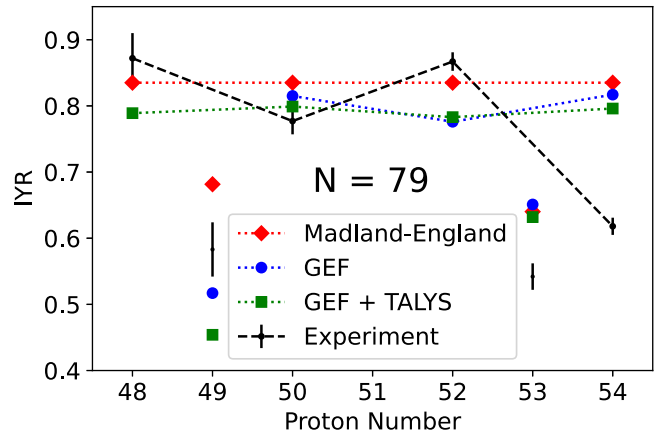

FIG. 13. The IYRs as a function of the proton number for the $N = 79$ isotones. The dotted lines connect isotones for which the spin-parity of the two states is the same.

V. CONCLUSIONS AND OUTLOOK

19 new isomeric yield ratios in 25-MeV ^{238}U(p, f) have been reported and, together with ratios from a previous measurement, compared with model calculations. The ratios show a large variation, from 0.27 to 0.98, some of which can be explained by the difference in spins between the isomers. However, it is observed that the ratios also vary between isomers with the same spin-parity, and even between isomers with similar nuclear structures. This shows that other factors than the fissioning system and the nuclear structure of the fragments play an important role in the population of the states. The systematic trends observed in the IYRs of close-lying isotopes and isotones with similar nuclear configuration suggests that the angular moment of the corresponding FFs also vary. This highlights the possibility to study angular momentum sharing in nuclear fission through IYR measurements.

The failure of the Madland-England model to reproduce the observed trends in the data supports the claims by Sears

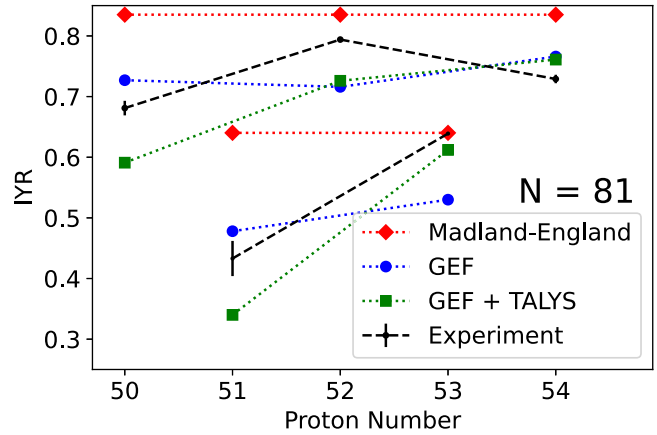

FIG. 14. The IYRs as a function of the proton number for the $N = 81$ isotones. The dotted lines connect isotones for which the spin-parity of the two states is the same.

et al. [41], that the assumption that the root-mean-square angular momentum is constant for all fission fragments of the same fission reaction is wrong. Furthermore, the failure of the model to get the average IYR correct for fission products with the same spin-parity of the states indicates that also the model's method of populating these states is wrong, or at least needs adjustment.

The large variation observed in the measured IYRs also supports the recent finding by Wilson *et al.* [43], that the average angular momentum of the fragments is strongly mass-dependent. In Wilson *et al.*, a saw-tooth behavior of the angular momentum as a function of mass number is observed. In our case, the mass numbers of the observed FPs do not span a large enough range to confirm this. Instead, the systematic trends observed in the IYRs of neighboring nuclides indicate a sort of fine structure behavior in the angular momentum of the FFs.

As described in the manual of GEF [13], the model and its parameters have been adjusted to available experimental data. Thus, the GEF model heavily relies on measured observables from fission. For proton-induced fission, very few experimental values have been published and used in the optimization. This could be one of the reasons for the observed discrepancies between the calculated and measured IYRs, as proton-induced fission is believed to increase the average angular momentum of the fissioning system. The discrepancies indicate that the empirical information from other types of fission, for example, spontaneous fission and thermal neutron-induced fission, is not sufficient to describe proton-induced fission. Hence, more data on IYR, as well as other observables, from proton-induced fission are needed to optimize the GEF model.

The combination of GEF+TALYS resulted in smaller IYRs than standalone GEF in almost all cases. This could possibly be attributed to the fact that TALYS, as opposed to GEF, removes angular momentum during the prompt de-excitation of the primary fission fragments, which leads to more population of the low-spin states and smaller IYRs. GEF has likely been optimized assuming no angular momentum removal due to neutron emission. This would lead to an underestimation of the IYR from TALYS when feeding it with the spin-energy matrix from GEF. Another possible reason for this mismatch could be that the spin cut-off parameter in the level densities of TALYS has not been properly fine-tuned for the fission fragment regime. As a conclusion, if GEF is to be used as a fission generator for the Hauser-Feshbach formalism of TALYS, as suggested by Fujio *et al.* [44], the spins of the primary fragments will have to be optimized fragment by fragment.

A first step in this direction, to develop a surrogate model that can be used to vary the input to TALYS based on GEF predictions, has been taken and will be presented in a forthcoming paper. In this model, the spin-energy matrix describing the excited FF is parametrized, and the parameter determining the angular momentum distribution is optimized to reproduce the experimental IYRs. Furthermore, the model takes into consideration all FFs that after neutron emission contribute to the population of the long-lived states of a particular FP. Thanks to the data set presented here, with systematic measurements of IYR of neighboring nuclides, the parameters can be optimized individually for each fragment to address the variation of angular momentum between the primary fragments.

ACKNOWLEDGMENTS

This work was supported by the Swedish research council Vetenskapsrådet (Ref. No. 2017-06481), the European Commission within the Seventh Framework Programme through Fission-2013-CHANDA (Project No. 605203), the Swedish Radiation Safety Authority (SSM), and the Swedish Nuclear Fuel and Waste Management Co. (SKB). Funding from the European Union's Horizon 2020 research and innovation program under Grant Agreement No. 771036 (ERC CoG MAIDEN) is gratefully acknowledged. The support from the Academy of Finland Projects No. 275389, No. 295207, No. 306980, No. 312544, and No. 327629 are acknowledged.

[1] *Compilation and Evaluation of Fission Yield Nuclear Data*, Final report of a co-ordinated research project 1991–1996 (International Atomic Energy Agency, Wagramer Strasse 5, P.O. Box 100, A-1400 Vienna, Austria, 2000).

[2] D. G. Sarantites, G. E. Gordon, and C. D. Coryell, Ratios of independent yields of the isomers $Te^{131-131m}$ and $Te^{133-133m}$ in fission, Phys. Rev. **138**, B353 (1965).

[3] N. Imanishi, I. Fujiwara, and T. Nishi, Independent isomer yields of Sb and Te isotopes in thermal-neutron fission of ^{233}U, ^{235}U and ^{239}Pu, Nucl. Phys. A **263**, 141 (1976).

[4] D. C. Aumann and W. Gückel, Absolute cross sections and isomeric cross-section ratios for the ^{148}Nd$(d, 2n)$, ^{148}Nd(p, n), ^{146}Nd(α, pn), Phys. Rev. C **16**, 160 (1977).

[5] I. Fujiwara, N. Imanishi, and T. Nishi, Isomer-yield rations and primary angular momenta of I, Xe and Cs isotopes produced in thermal-neutron fission of ^{233}U, ^{235}U and ^{239}Pu, J. Phys. Soc. Jpn. **51**, 1713 (1982).

[6] G. P. Ford, K. Wolfsberg, and B. R. Erdal, Independent yields of the isomers of ^{133}Xe and ^{135}Xe for neutron-induced fission of ^{233}U, ^{235}U, ^{238}U, and ^{242}Am^m, Phys. Rev. C **30**, 195 (1984).

[7] V. Rakopoulos *et al.*, First isomeric yield ratio measurements by direct ion counting and implications for the angular momentum of the primary fission fragments, Phys. Rev. C **98**, 024612 (2018).

[8] V. Rakopoulos *et al.*, Isomeric fission yield ratios for odd-mass cd and in isotopes using the phase-imaging ion-cyclotron-resonance technique, Phys. Rev. C **99**, 014617 (2019).

[9] T. Kajino *et al.*, Current status of r-process nucleosynthesis, Prog. Part. Nucl. Phys. **107**, 109 (2019).

[10] M. Arnould, S. Goriely, and K. Takahashi, The r-process of stellar nucleosynthesis: Astrophysics and nuclear physics achievements and mysteries, Phys. Rep. **450**, 97 (2007).

[11] A. A. Sonzogni, T. D. Johnson, and E. A. McCutchan, Nuclear structure insights into reactor antineutrino spectra, Phys. Rev. C **91**, 011301(R) (2015).

[12] M. Gupta, M. A. Kellett, A. L. Nichols, O. Bersillon, Assessment of fission product decay data requirements for Th/U fuel. Tech. rep., IAEA report INDC(NDS)-0577, IAEA, Vienna, Austria, May 2010. Also available online https://nds.iaea.org/publications/indc/indc-nds-0577.pdf.

[13] K.-H. Schmidt, B. Jurado, C. Amouroux, and C. Schmitt, General description of fission observables: GEF model code, Nucl. Data Sheets **131**, 107 (2016).

[14] R. Capote *et al.*, RIPL – Reference input parameter library for calculation of nuclear reactions and nuclear data evaluations, Nucl. Data Sheets **110**, 3107 (2009).

[15] I. Stetcu, A. E. Lovell, P. Talou, T. Kawano, S. Marin, S. A. Pozzi, and A. Bulgac, Angular momentum removal by neutron and γ-ray emissions during fission fragment decays, Phys. Rev. Lett. **127**, 222502 (2021).

[16] D. G. Madland and T. R. England, The influence of isomeric states on independent fission product yields, Nucl. Sci. Eng. **64**, 859 (1977).

[17] A. Koning, S. Hilaire, and S. Goriely, TALYS: modeling of nuclear reactions, Euro. Phys. J. A **59**, 131 (2023).

[18] I. D. Moore *et al.*, Towards commissioning the new IGISOL-4 facility, Nucl. Instrum. Methods Phys. Res. B **317**, 208 (2013).

[19] S. Eliseev, K. Blaum, M. Block, C. Droese, M. Goncharov, E. Minaya Ramirez, D. A. Nesterenko, Y. N. Novikov, and L. Schweikhard, Phase-imaging ion-cyclotron-resonance measurements for short-lived nuclides, Phys. Rev. Lett. **110**, 082501 (2013).

[20] Z. Gao *et al.*, Applying machine learning methods for the analysis of two-dimensional mass spectra, Eur. Phys. J. A **59**, 169 (2023).

[21] T. Eronen *et al.*, JYFLTRAP a Penning trap for precision mass spectroscopy and isobaric purification, Eur. Phys. J. A **48**, 46 (2012).

[22] G. Savard *et al.*, A new cooling technique for heavy ions in a Penning trap, Phys. Lett. A **158**, 247 (1991).

[23] S. Eliseev *et al.*, A phase-imaging technique for cyclotron-frequency measurements, Appl. Phys. B **114**, 107 (2014).

[24] D. A. Nesterenko *et al.*, Phase-imaging ion-cyclotron-resonance technique at the JYFLTRAP double Penning trap mass spectrometer, Eur. Phys. J. A **54**, 154 (2018).

[25] D. Nesterenko *et al.*, Study of radial motion phase advance during motion excitations in a Penning trap and accuracy of JYFLTRAP mass spectrometer, Eur. Phys. J. A **57**, 302 (2021).

[26] I. Stetcu, P. Talou, T. Kawano, and M. Jandel, Properties of prompt-fission γ rays, Phys. Rev. C **90**, 024617 (2014).

[27] P. Talou, T. Kawano, and I. Stetcu, Prompt fission neutrons and γ rays, Nucl. Data Sheets **118**, 195 (2014).

[28] O. Litaizea, O. Serot, and L. Berge, Fission modelling with FIFRELIN, Eur. Phys. J. A **51**, 177 (2015).

[29] J. Verbeke, J. Randrupb, and R. Vogt, Fission reaction event yield algorithm, FREYA − For event-by-event simulation of fission, Comput. Phys. Commun. **191**, 178 (2015).

[30] W. Hauser and H. Feshbach, The inelastic scattering of neutrons*, Phys. Rev. **87**, 366 (1952).

[31] J. R. Huizenga and R. Vandenbosch, Interpretation of isomeric cross-section ratios for (n,γ) and (γ,n) reactions, Phys. Rev. **120**, 1305 (1960).

[32] R. Vandenbosch and J. R. Huizenga, Isomeric cross-section ratios for reactions producing the isomeric pair Hg-197, Hg-197m, Phys. Rev. **120**, 1313 (1960).

[33] A. Al-Adili, V. Rakopoulos, and A. Solders, Extraction of angular momenta from isomeric yield ratios, Eur. Phys. J. A **55**, 61 (2019).

[34] W. Dilg, W. Schantl, and H. Vonach, Level density parameters for the back-shifted fermi gas model in the mass range 40 $<$ A $<$ 250, Nucl. Phys. A **217**, 269 (1973).

[35] F. G. Kondev *et al.*, The NUBASE2020 evaluation of nuclear properties, Chin. Phys. C **45**, 030001 (2021).

[36] D. Nesterenko *et al.*, Three beta-decaying states in ^{128}In and ^{130}In resolved for the first time using Penning-trap techniques, Phys. Lett. B **808**, 135642 (2020).

[37] C. Izzo *et al.*, Mass measurements of neutron-rich indium isotopes for r-process studies, Phys. Rev. C **103**, 025811 (2021).

[38] L. Limura, J. Katakura, and S. Ohya, Nuclear data sheets for A = 126*, Nucl. Data Sheets **180**, 1 (2022).

[39] K. Sieglv, K. Kolos, N. D. Scielzo, A. Aprahamian, G. Savard, M. T. Burkey, M. P. Carpenter, P. Chowdhury, J. A. Clark, P. Copp, G. J. Lane, C. J. Lister, S. T. Marley, E. A. McCutchan, A. J. Mitchell, J. Rohrer, M. L. Smith, and S. Zhu, β-decay half-lives of ^{134,134m}Sb and their isomeric yield ratio produced by the spontaneous fission of ^{252}Cf, Phys. Rev. C **98**, 054307 (2018).

[40] From ENSDF database as of April 05, 2022, version available at http://www.nndc.bnl.gov/ensarchivals/.

[41] C. Sears *et al.*, Compilation and evaluation of isomeric fission yield ratios, Nucl. Data Sheets **173**, 118 (2021).

[42] V. Guadilla *et al.*, Large impact of the decay of niobium isomers on the reactor $\bar{\nu}_e$ summation calculations, Phys. Rev. Lett. **122**, 042502 (2019).

[43] J. Wilson *et al.*, Angular momentum generation in nuclear fission, Nature (London) **590**, 566 (2021).

[44] K. Fujio *et al.*, TALYS calculations of prompt fission observables and independent fission product yields for the neutron-induced fission of ^{235}U, Eur. Phys. J. A **59**, 178 (2023).